J. Fluid Mech. (2022), vol. 933, A8, doi:10.1017/jfm.2021.1057

The logarithmic variance of streamwise velocity and k^{-1} conundrum in wall turbulence

Yongyun Hwang[1],†, **Nicholas Hutchins**[2] **and Ivan Marusic**[2]

[1]Department of Aeronautics, Imperial College London, South Kensington SW7 2AZ, UK

[2]Department of Mechanical Engineering, University of Melbourne, Victoria 3010, Australia

(Received 25 October 2021; revised 25 October 2021; accepted 23 November 2021)

The logarithmic dependence of streamwise turbulence intensity has been observed repeatedly in recent experimental and direct numerical simulation data. However, its spectral counterpart, a well-developed k^{-1} spectrum (k is the spatial wavenumber in a wall-parallel direction), has not been convincingly observed from the same data. In the present study, we revisit the spectrum-based attached eddy model of Perry and co-workers, who proposed the emergence of a k^{-1} spectrum in the inviscid limit, for small but finite z/δ and for finite Reynolds numbers (z is the wall-normal coordinate, and δ is the outer length scale). In the upper logarithmic layer (or inertial sublayer), a reexamination reveals that the intensity of the spectrum must vary with the wall-normal location at order of z/δ, consistent with the early observation argued with 'incomplete similarity'. The streamwise turbulence intensity is subsequently calculated, demonstrating that the existence of a well-developed k^{-1} spectrum is not a necessary condition for the approximate logarithmic wall-normal dependence of turbulence intensity – a more general condition is the existence of a premultiplied power-spectral intensity of $O(1)$ for $O(1/\delta) < k < O(1/z)$. Furthermore, it is shown that the Townsend–Perry constant must be weakly dependent on the Reynolds number. Finally, the analysis is semi-empirically extended to the lower logarithmic layer (or mesolayer), and a near-wall correction for the turbulence intensity is subsequently proposed. All the predictions of the proposed model and the related analyses/assumptions are validated with high-fidelity experimental data (Samie *et al.*, *J. Fluid Mech.*, vol. 851, 2018, pp. 391–415).

Key words: turbulence theory, turbulent boundary layers

† Email address for correspondence: y.hwang@imperial.ac.uk

1. Introduction

Despite the debate on its precise form, the logarithmic profile for mean velocity has been understood as the most fundamental feature of wall-bounded turbulence (von Kármán 1930). The attached eddy hypothesis of Townsend (1956, 1976) was built upon this feature and states the possible existence of energy-containing motions, the size of which is proportional to their distance from the wall (i.e. attached eddies) (see also Hwang & Lee 2020, for the theoretical basis of the hypothesis). Townsend (1956, 1976) subsequently introduced a generic form of the second-order statistical moments of the individual energy-containing eddies under the assumption that they behave 'inviscidly' as in a Biot–Savart model in the region close to the wall: i.e. a slip boundary condition is considered for the wall-parallel velocity components, while the no-penetration condition is imposed on the wall-normal velocity. He then showed that linear superposition of the second-order statistical moments subject to constant Reynolds shear stress leads to

$$\frac{\overline{u'u'}}{u_\tau^2} = -A \ln\left(\frac{z}{\delta}\right) + B, \tag{1.1}$$

where u' is the streamwise turbulent velocity fluctuation, u_τ is the friction velocity, z is the wall-normal coordinate, δ is the outer length scale (e.g. half height of channel, radius of pipe and thickness of boundary layer), A is the Townsend–Perry constant and B is a constant. Several important refinements of the original theory of Townsend (1956, 1976) were subsequently made. These include: (1) the description of the logarithmic mean velocity in terms of the mean vorticity of individual attached eddies (e.g. Perry & Chong 1982; Perry, Henbest & Chong 1986); (2) the prescription of a more realistic statistical form of the individual attached eddy (Perry & Chong 1982; Perry *et al.* 1986; Woodcock & Marusic 2015); (3) relating the physical-space model of Townsend (1956, 1976) to k^{-1} behaviour in velocity spectra (k is the spatial wavenumber in a wall-parallel direction) (Perry & Chong 1982; Perry *et al.* 1986); (4) the empirical extensions to the near-wall region (Marusic & Kunkel 2003); and (5) the generalisation of (1.1) for higher-order turbulence statistics (Meneveau & Marusic 2013).

Over the past two decades, a substantial amount of evidence supporting the attached eddy hypothesis and related models has emerged (see also Marusic & Monty 2019). For example, laboratory experiments and numerical simulations have repeatedly confirmed that (1.1) is indeed a first approximation to the streamwise and spanwise turbulence intensities in the logarithmic layer (Jiménez & Hoyas 2008; Hultmark *et al.* 2012; Marusic *et al.* 2013; Lee & Moser 2015; Baars & Marusic 2020*b*). The existence and the statistical structure of self-similar energy-containing motions in the logarithmic layer have also been reported with various types of eddy-extraction techniques (del Álamo *et al.* 2006; Hwang & Cossu 2011; Lozano-Durán & Jiménez 2014; Hwang 2015; Hellstöm, Marusic & Smits 2016; Hwang & Bengana 2016; Hwang & Sung 2018; Cheng *et al.* 2019; Baars & Marusic 2020*a*). Finally, mathematical analyses of the Navier–Stokes equations have consistently revealed that the key feature of the logarithmic layer is self-similarity with the distance from the wall, which underpins the scaling of the mean, linear and nonlinear dynamics (del Álamo & Jiménez 2006; Hwang & Cossu 2010; Klewicki 2013; Moarref *et al.* 2013; Hwang 2016; Hwang, Willis & Cossu 2016; McKeon 2017; Eckhardt & Zammert 2018; Doohan, Willis & Hwang 2019; McKeon 2019; Vadarevu *et al.* 2019; Yang, Willis & Hwang 2019; Hwang & Eckhardt 2020; Hwang & Lee 2020; Skouloudis & Hwang 2021).

Despite the growing evidence, the description of velocity spectra in terms of the attached eddy models still remains unsettled. In the earliest work (Perry & Chong 1982; Perry *et al.* 1986), it was proposed that the existence of a k^{-1} spectrum with the intensity of A in

https://doi.org/10.1017/jfm.2021.1057 Published online by Cambridge University Press

(1.1) would be consistent with the logarithmic wall-normal dependence of streamwise turbulence intensity (see also § 2.1). In particular, the inviscid theory of Perry *et al.* (1986) showed that such a k^{-1} spectrum would emerge in the region where the spectrum is expected to scale simultaneously in z and δ. However, early measurements from the Princeton Superpipe did not show a clearly discerned k^{-1} spectrum, and this was subsequently postulated as a consequence of 'incomplete similarity' by arguing that the simultaneous scaling with z and δ may not be possible (Morrison *et al.* 2001, 2004). It was later suggested that a well-developed k^{-1} spectrum could appear in the location closer to the wall (Nickels *et al.* 2005), although the proposed location is too close to the wall to directly relate to (1.1), which typically appears in the upper logarithmic layer (Marusic *et al.* 2013; Vallikivi, Hultmark & Smits 2015; Vassilicos *et al.* 2015), i.e. $O(Re_\tau^{-1/2}) \lesssim y/\delta \lesssim 0.15$ ($Re_\tau = u_\tau\delta/\nu$ is the friction Reynolds number, where ν is the kinematic viscosity) or the layer just above the 'mesolayer' (Afzal 1982; Sreenivasan & Sahay 1997; Wei *et al.* 2005; Klewicki 2013). Furthermore, it was recently suggested that a well-visible k^{-1} spectrum responsible for (1.1) might appear at least for $Re_\tau \gtrsim 8 \times 10^4$ (Samie *et al.* 2018; Baars & Marusic 2020*a*). In this respect, it should finally be mentioned that an alternative form of k^{-1} spectrum was also recently proposed by Srinath *et al.* (2018) based on a space-filling argument of energy-containing motions, although their model does not necessarily rely on the existence of self-similar energy-containing motions (i.e. attached eddy hypothesis).

The objective of the present study is to propose a spectrum-based attached eddy model that integrates the seemingly inconsistent observations listed above into a single framework. To this end, we revisit the spectrum-based attached eddy model of Perry *et al.* (1986), which is based on the work of Perry & Abel (1977). We re-examine the underlying assumptions in the model with the high-fidelity experimental data from Samie *et al.* (2018). We subsequently extend the model for small but finite z/δ and finite Reynolds number, so that its application becomes directly suitable to the location where (1.1) has been observed (layer I in figure 2). The examination reveals that, in general, the intensity of the spectrum for $1/\delta \ll k \ll 1/z$ must vary with the wall-normal direction at $O(z/\delta)$ without assuming a well-developed k^{-1} spectrum. The presence of such a complicated spectrum in the absence of a k^{-1} spectrum is, however, found not to affect the form of streamwise turbulence intensity in (1.1) significantly – indeed, the Townsend–Perry constant A is found to be only weakly dependent on the Reynolds number due to viscous wall effects. The theoretical framework is further extended to the mesolayer (layer II in figure 2), and a near-wall correction is subsequently proposed. The theoretical developments made in the present study are validated with the high-fidelity experimental data of Samie *et al.* (2018).

2. Background

2.1. *The original model*

We first revisit the original spectrum-based attached eddy model of Perry *et al.* (1986), focusing on the streamwise velocity in a turbulent boundary layer, the thickness of which is given by δ. The modelling efforts start with the streamwise turbulence intensity given in terms of the power-spectral density:

$$\overline{u'u'}(z) = \int_0^\infty \Phi_{uu}(k_x, z)\, \mathrm{d}k_x, \tag{2.1}$$

where $\Phi_{uu}(k_x, z)$ is the power-spectral density of streamwise velocity at each wall-normal location z, and k_x is the streamwise wavenumber. As in Townsend (1976), only the flow

https://doi.org/10.1017/jfm.2021.1057 Published online by Cambridge University Press

above the thin viscous sublayer was considered, assuming that the flow is inviscid with finite slip velocity at the boundary. Under this assumption, the power-spectral density Φ_{uu} is expected to be a function of u_τ, k_x, z and δ. Further to this, $z \ll \delta$ was assumed, given the wall-normal location of interest (i.e. the logarithmic layer).

Under the two assumptions (i.e. $Re_\tau \to \infty$ and $z \ll \delta$), the model yields a power-spectral density of streamwise velocity schematically depicted in figure 1. At a given wall-normal location $z \ll \delta$, energy-containing eddies of outer scale would contribute to the wavenumbers of $k_x \sim O(1/\delta)$ through their inactive component (Perry & Abel 1977; Perry *et al.* 1986). In this range of wavenumbers, the assumption of $z \ll \delta$ implies that the power-spectral density can further be assumed to be independent of z/δ. Using (2.1), the power-spectral density for $k_x \sim O(1/\delta)$ is then given by

$$\frac{\Phi_{uu}(k_x, z)}{u_\tau^2} = \frac{\delta\, \Phi_{uu}(k_x\delta)}{u_\tau^2} = \delta\, g_1(k_x\delta). \tag{2.2a}$$

The premultiplied power-spectral density is subsequently written as

$$\frac{k_x\, \Phi_{uu}(k_x, z)}{u_\tau^2} = k_x\delta\, g_1(k_x\delta) = h_1(k_x\delta), \tag{2.2b}$$

as sketched in the δ-scaling region of figure 1. For the wavenumbers of $k_x \sim O(1/z)$, the power-spectral density would not be a function of δ, as only eddies scaling in z would contribute to these wavenumbers. Therefore, at $z \ll \delta$, the power-spectral density for $k_x \sim O(1/z)$ becomes

$$\frac{\Phi_{uu}(k_x, z)}{u_\tau^2} = \frac{z\, \Phi_{uu}(k_x z)}{u_\tau^2} = z\, g_2(k_x z), \tag{2.3a}$$

and the corresponding premultiplied power-spectral density is

$$\frac{k_x\, \Phi_{uu}(k_x, z)}{u_\tau^2} = k_x z\, g_2(k_x z) = h_2(k_x z). \tag{2.3b}$$

This is sketched in the z-scaling region in figure 1. The power spectrum for very high k_x should obviously be related to the energy cascade (the Kolmogrov scaling region in figure 1). Therefore it follows the scaling of inertial subrange ($k_x^{-5/3}$ spectrum) and the dissipation at the Kolmogorov length scale η (Perry *et al.* 1986). The details of this part of the spectrum will not, however, be pursued here because its contribution to turbulence intensity would be small.

We now consider the wavenumber region of $1/\delta \ll k_x \ll 1/z$ (the overlap region in figure 1). In this region, it was argued that both of the scalings in (2.2*b*) and (2.3*b*) would simultaneously be valid. Here, note that h_1 in (2.2*b*) is a function of only $k_x\delta$, while h_2 in (2.3*b*) is a function of $k_x z$. Therefore matching between (2.2*b*) and (2.3*b*) leads to

$$h_1(k_x z) = h_2(k_x\delta) = A, \tag{2.4}$$

where A is a constant independent of both $k_x z$ and $k_x\delta$, resulting in the following power spectrum:

$$\frac{\Phi_{uu}(k_x, z)}{u_\tau^2} = \frac{A}{k_x}. \tag{2.5}$$

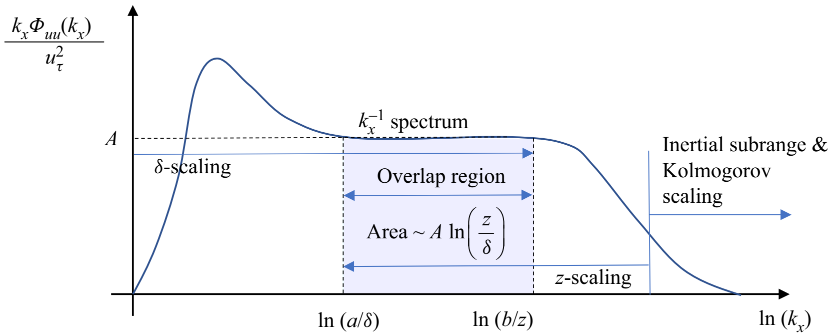

Figure 1. A schematic diagram of the streamwise velocity spectrum for the attached eddy model of Perry *et al.* (1986). Here, the overlap region (i.e. inertial subrange) between z-scaling and dissipation (Kolmogorov) scaling and the dissipation scaling region are merged into a single region for simplicity (see text). Note that this is only a conceptual sketch introduced to explain the model of Perry *et al.* (1986). Therefore it does not necessarily reflect the experimentally measured spectrum of streamwise velocity, especially when the Reynolds number is not sufficiently high.

Using (2.1), (2.2*b*), (2.3*b*) and (2.5), the streamwise turbulence intensity, which is the area below the curve for the power-spectral density in figure 1, is obtained as

$$\begin{aligned}\frac{\overline{u'u'}}{u_\tau^2} &= \int_{-\infty}^{\infty} \frac{k_x\,\Phi_{uu}(k_x;z)}{u_\tau^2}\,\mathrm{d}(\ln k_x) = \int_{\ln(a/\delta)}^{\ln(b/z)} \frac{k_x\,\Phi_{uu}(k_x)}{u_\tau^2}\,\mathrm{d}(\ln k_x) + C(z;Re_\tau)\\ &= -A\ln\left(\frac{z}{\delta}\right) + B(z;Re_\tau),\end{aligned} \tag{2.6a}$$

where a and b are the constants defining the wavenumber boundaries of the k_x^{-1} region (blue-shaded region in figure 1) and

$$B(z;Re_\tau) = A\ln\left(\frac{a}{b}\right) + C(z;Re_\tau), \tag{2.6b}$$

$$C\,(z;Re_\tau) = \frac{\overline{u'u'}}{u_\tau^2} - \int_{\ln(a/\delta)}^{\ln(b/z)} \frac{k_x\,\Phi_{uu}(k_x)}{u_\tau^2}\,\mathrm{d}(\ln k_x). \tag{2.6c}$$

Here, $C(z;Re_\tau)$ depicts the contribution from the remainder of the latter integral in (2.6*a*), and it should be a weak function of z and Re_τ due to the small contribution made from the Kolmogorov-scaling part of the spectrum. (Note that under the original assumptions of Perry *et al.* (1986), the contribution from the outer-scaling part for $k_x \le a/\delta$ to $C(z;Re_\tau)$ does not depend on z and Re_τ; see (2.2*a*).) If this contribution is ignored, then B and C become constants, leading (2.6*a*) to be identical to (1.1) from Townsend (1976). We note that (1.1) in Townsend (1976) was obtained by ignoring the contribution from small-scale eddies for energy cascade and dissipation. Therefore the two models by Townsend (1976) and by Perry *et al.* (1986), the former of which was built in physical space and the latter in spectral space, become consistent.

2.2. *Scaling of streamwise velocity spectra*

Now we examine the spectrum-based attached eddy model of Perry *et al.* (1986) using the experimental data from Samie *et al.* (2018). These data were taken from the high Reynolds number boundary layer wind tunnel located at the University of Melbourne.

The boundary-layer thickness δ and friction velocity u_τ were estimated by fitting the measured experimental data to a composite law of the wall/wake curve in Chauhan, Monkewitz & Nagib (2010). Samie *et al.* (2018) compared their estimates for u_τ from the composite fit to those measured directly by Baars *et al.* (2016) with a floating element drag balance, in the same facility, and matched x and U_∞ (free-stream velocity) to the two highest Reynolds numbers of Samie *et al.* (2018), finding agreement to within $\pm 1\%$ The near-wall region is fully resolved using the nanoscale thermal anemometry probes (NSTAPs) (Vallikivi & Smits 2014). The Reynolds numbers considered are $Re_\tau = 6123, 10\,100, 14\,680, 19\,680$. For further details on the experiment, the reader may refer to Samie *et al.* (2018).

Figure 2 shows the contours of the premultiplied streamwise power-spectral density of streamwise velocity at $Re_\tau = 19\,680$, in which the two red straight lines indicate $\lambda_x = z$ and $\lambda_x = 10\delta$. We first define the conventional logarithmic layer with a relatively conservative limit: $z \in [z_i, z_o]$ where $z_i^+ = 200$ and $z_o = 0.1\delta$ (the superscript $^+$ denotes the normalisation with $\delta_\nu (= \nu/u_\tau)$ and u_τ). As was proposed previously (Afzal 1982; Sreenivasan & Sahay 1997; Wei *et al.* 2005; Klewicki 2013), the logarithmic layer may be partitioned further into two sublayers with the boundary at $z_m^+ = 3.6 Re_\tau^{1/2}$: i.e. layer I for $z \in [z_m, z_o]$, and layer II for $z \in [z_i, z_m]$. Here, we note that the location of z_m is a little below the empirical wall-normal location of the outer peak in the spectra ($z_m^+ = 3.9 Re_\tau^{1/2}$) proposed by Mathis, Hutchins & Marusic (2009).

(i) Layer I (inertial sublayer): in this layer, the inertial effect would dominate the viscous wall effect. Given the inviscid-flow assumption of Perry *et al.* (1986), this is the location where their model is supposed to be directly applicable. Indeed, the contour lines for $\lambda_x \gtrsim 10\delta$ in figure 2 change little along the z-direction and remain mostly parallel to $\lambda_x = 10\delta$, indicating that (2.2*b*) would be a good approximation for $\lambda_x \gtrsim 10\delta$. Similarly, the contour lines for $10^{-2}\delta \leq \lambda_x \leq \delta$ are approximately parallel to $\lambda_x = z$, consistent with (2.3*b*). These scaling behaviours are more precisely confirmed in figure 3 – the spectra in layer I follow the scaling of (2.2*b*) for $\lambda_x \gtrsim 10\delta$ (figure 3*a*) and they do so with (2.3*b*) for $z \lesssim \lambda_x \lesssim 10z$ (figure 3*b*). Despite the scaling behaviours being fully consistent with (2.2*b*) and (2.3*b*), the spectra in between ($10z \leq \lambda_x \leq 10\delta$) do not seem to exhibit a well-developed k_x^{-1} behaviour. Furthermore, the values of the spectra vary non-negligibly with z, indicating that there is an issue in comparing (2.5) with the experimental data (e.g. Morrison *et al.* 2001, 2004; Rosenberg *et al.* 2013). These issues will be discussed in depth in § 3.

(ii) Layer II (mesolayer): given the nature of the mean momentum balance in this layer (Afzal 1982; Sreenivasan & Sahay 1997; Wei *et al.* 2005; Klewicki 2013), the viscous wall effect would be more important than the inertial effect. In particular, the premultiplied power-spectral density for $\lambda_x \gtrsim 10\delta$ appears to become weaker as $z \to 0$, and the related contour lines in figure 2 are not parallel to $\lambda_x = 10\delta$. On the contrary, the power-spectral density for $10^{-2}\delta \leq \lambda_x \leq 10^{-1}\delta$ still appears to follow (2.3*b*), as the contour lines in figure 2 are approximately parallel to $\lambda_x = z$ (see also figure 7). This is also confirmed in figure 3 – the spectra in layer II do not precisely follow the scaling of (2.2*b*) for $\lambda_x \gtrsim 10\delta$ (figure 3*c*), while they show a behaviour consistent with (2.3*b*) for $z \lesssim \lambda_x \lesssim 10z$ (figure 3*d*). These observations will be the basis of the model for layer II in § 4, obtained by extending the one in § 3.

We note that the classification of the logarithmic layer into layers I and II in the present study is based on the streamwise velocity spectra, not on the mean velocity. Given the

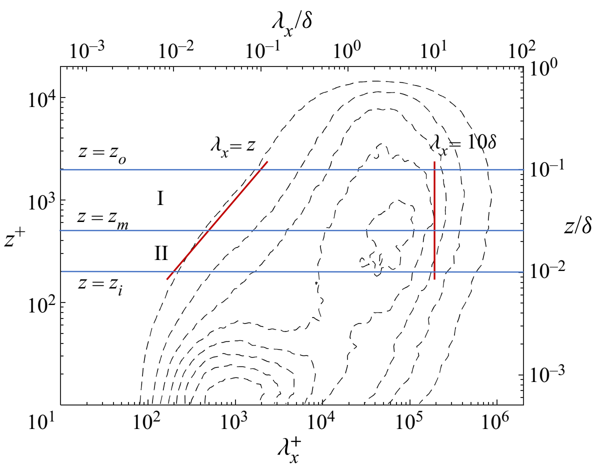

Figure 2. Premultiplied streamwise power-spectral density of streamwise velocity ($k_x^+ \Phi_{uu}^+(z; k_x)$) at $Re_\tau \simeq 19\,680$ (data from Samie *et al.* 2018). The contour lines are $k_x^+ \Phi_{uu}^+(z; k_x) = 0.25, 0.5, 0.75, 1, 1.25, 1.5, 1.75, 2.0$. Here, the logarithmic layer from $z^+ = 200$ to $z/\delta = 0.1$ is divided into two sublayers: layer I (inertial sublayer) and layer II (mesolayer). The two red solid lines indicate $\lambda_x = z$ and $\lambda_z = 10\delta$, as labelled.

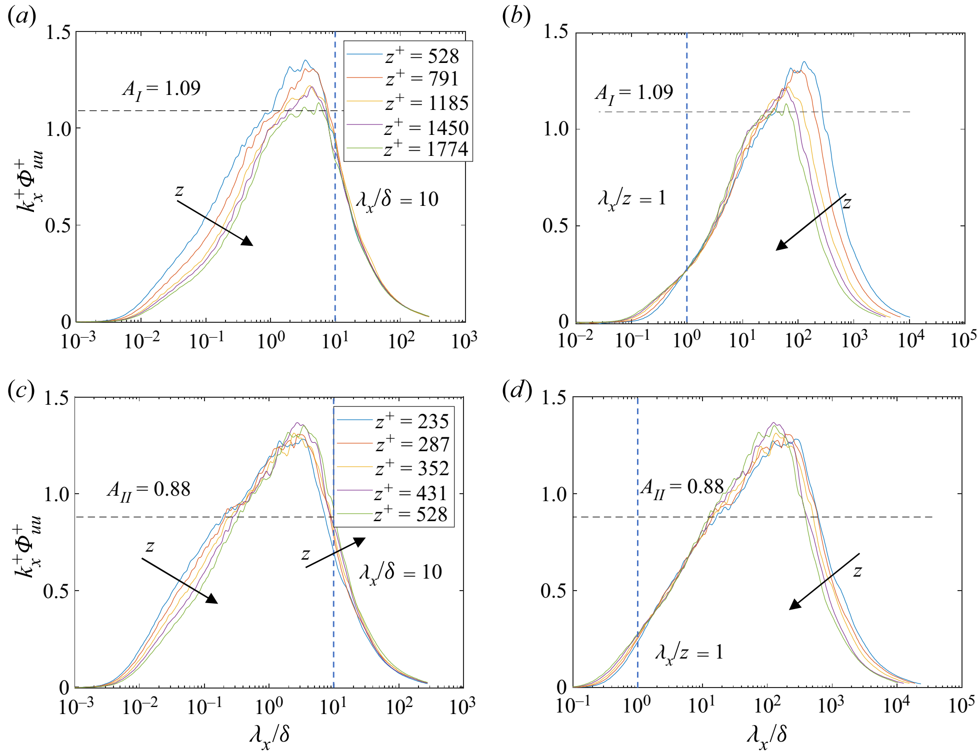

Figure 3. Premultiplied streamwise power-spectral density of streamwise velocity in (a,b) layer I and (c,d) layer II at $Re_\tau = 19\,680$: (a,c) δ-scaling, and (b,d) z-scaling. The arrows indicate the directions of increasing z.

streamwise mean momentum equation for a turbulent boundary layer, the streamwise mean velocity is mostly related to the Reynolds shear stress like channel and pipe flows. However, the fluctuations of the streamwise velocity carry a substantial amount of motions that contain little Reynolds shear stress. Such motions have been referred to as 'inactive' motions (Townsend 1976), which appear to be particularly important in the region close to the wall (Hwang 2015, 2016; Cho, Hwang & Choi 2018; Baars & Marusic 2020*a*; Deshpande, Monty & Marusic 2020). These motions do not necessarily have strong effect on the mean velocity. Therefore the empirical scaling of $z_m^+ (= 3.6Re_\tau^{1/2})$ used here is not necessarily the same as the wall-normal location (say z_R) that has been used to partition the inertial sublayer and the mesolayer based on the Reynolds shear stress (i.e. z_R is the location where the Reynolds shear stress is maximum). Indeed, an empirical value of z_R^+ is given by $z_R^+ = 1.9Re_\tau^{1/2}$ (Afzal & Yajnik 1973; Afzal 1976, 1982; Sreenivasan & Sahay 1997; Wei *et al.* 2005; Jiménez & Moser 2007; Klewicki 2013), indicating that $z_m > z_R$. This implies that the Reynolds shear stress would slightly decrease with z in layer I and that the peak Reynolds shear stress is located in layer II.

3. Proposed model

We first consider layer I, where the scalings in (2.2*b*) and (2.3*b*) were found to be consistent with the experimental data. The inviscid flow assumption of Perry *et al.* (1986) would still be applicable because the streamwise velocity is not zero at the lower boundary of layer I ($z = z_m$). However, the assumption of $z \ll \delta$ needs to be dealt with more carefully, if the Reynolds number is not infinite. Indeed, even at the highest Reynolds number considered in Samie *et al.* (2018) ($Re_\tau = 19\,680$), $z_m \simeq 0.025\delta$ and $z_o = 0.1\delta$. Therefore, in layer I, the value of z/δ is not infinitesimal, but only small and finite with z/δ varying from $O(Re_\tau^{-1/2})$ to $O(10^{-1})$. This implies that the assumption of $z \ll \delta$ in Perry *et al.* (1986) would not strictly be valid in most of layer I even at $Re_\tau = 19\,680$.

3.1. *Spectrum at* $1/\delta \ll k_x \ll 1/z$ *for small and finite* z/δ

If z/δ is finite in the region of interest, then the power-spectral density for $k_x \sim O(1/\delta)$ and $k_x \sim O(1/z)$ would not strictly be independent of z/δ. Such a behaviour is particularly pronounced in the region above layer I where z/δ is not small: indeed, the contour lines of the premultiplied spectra in figure 2 are not parallel to $\lambda_x = 10\delta$ and $\lambda_x = z$. Therefore, without loss of generality, the premultiplied spectra in (2.2*b*) and (2.3*b*) should be replaced with

$$\frac{k_x\, \Phi_{uu}(k_x, z)}{u_\tau^2} = \frac{k_x\delta\, \Phi_{uu}(k_x\delta, z/\delta)}{u_\tau^2} = \tilde{h}_1\left(k_x\delta, \frac{z}{\delta}\right) \tag{3.1a}$$

and

$$\frac{k_x\, \Phi_{uu}(k_x, z)}{u_\tau^2} = \frac{k_x z\, \Phi_{uu}(k_x z, z/\delta)}{u_\tau^2} = \tilde{h}_2\left(k_x z, \frac{z}{\delta}\right), \tag{3.1b}$$

respectively. Considering a z/δ-dependence of the spectrum for $k_x \sim O(1/\delta)$ and $k_x \sim O(1/z)$ is physically more sound and offers more modelling flexibility. Indeed, (3.1*a*) would allow one to account for any wall-normal variation of outer-scaling structures such as superstructures/very-large-scale motions, while (3.1*b*) allows one to consider directly the small wall-normal variation in the z-scaling spectrum caused by the energy cascade.

Now (3.1*a*) and (3.1*b*) are considered for $1/\delta \ll k_x \ll 1/z$. For $1/\delta \ll k_x \ll 1/z$, the spectrum should satisfy $\tilde{h}_1(k_x\delta, z/\delta) = \tilde{h}_2(k_x z, z/\delta)$. Here, $k_x z$ and $k_x\delta$ must be treated as

https://doi.org/10.1017/jfm.2021.1057 Published online by Cambridge University Press

two independent variables, because the two scaling laws in (3.1*a*) and (3.1*b*) from the Buckingham π theorem are introduced to cover different values of k_x at all admissible small z/δ (Hinch 1991). While this may be a useful feature to proceed further to identify the form of spectrum for $1/\delta \ll k_x \ll 1/z$, here we shall write the following form of the premultiplied spectrum without loss of generality:

$$\frac{k_x\,\Phi_{uu}(k_x, z)}{u_\tau^2} = h\left(k_x l_I, \frac{z}{\delta}\right), \tag{3.2}$$

leading to

$$\frac{\Phi_{uu}(k_x, z)}{u_\tau^2} = \frac{h(k_x l_I, z/\delta)}{k_x}, \tag{3.3}$$

where l_I is an appropriate length scale that can be chosen for $z \ll l_I \ll \delta$ in the range of $1/\delta \ll k_x \ll 1/z$. Here, we note that only the condition of $z/\delta \to 0$ is relaxed compared to Perry *et al.* (1986), as we are concerned with finite Reynolds number and turbulence intensity for layer I. While we assume that there is no explicit form of the spectrum available for $1/\delta \ll k_x \ll 1/z$, the form of (3.3) raises several non-trivial issues to be discussed as follows.

(i) The spectrum for $O(1/\delta) < k_x < O(1/z)$: while (3.3) provides a general form of the spectrum for $1/\delta \ll k_x \ll 1/z$, this part of the spectrum should not be interpreted as an outcome of simultaneous 'physical' contribution of δ- and z-scaling motions, as was argued in Perry *et al.* (1986). We note that the logarithmic wall-normal dependence of the u variance in the original theory of Townsend (1976) is due to the wall-reaching inactive motions of each attached eddy, the size of which varies from $O(z)$ to $O(\delta)$. In other words, the non-zero spectrum for $O(1/\delta) < k_x < O(1/z)$ should be primarily from the contribution of the inactive motions of those attached eddies, as was also directly confirmed by the recent work of Deshpande *et al.* (2020).

(ii) Relation to the original model: now let us assume $Re_\tau \to \infty$, so that the lower boundary of layer I reaches the wall (i.e. $z_m \to 0$). In this case, using the Taylor series expansion about $z = 0$, the premultiplied power-spectral intensity in (3.1*a*), (3.1*b*) and (3.3) can further be approximated with

$$\tilde{h}_1(k_x\delta, z/\delta) = \tilde{h}_1(k_x\delta, 0) + \frac{\partial \tilde{h}_1(k_x\delta, 0)}{\partial(z/\delta)}\left(\frac{z}{\delta}\right) + O\left(\frac{z^2}{\delta^2}\right) \tag{3.4a}$$

for $k_x \sim O(1/\delta)$,

$$\tilde{h}_2(k_x z, z/\delta) = \tilde{h}_2(k_x z, 0) + \frac{\partial \tilde{h}_2(k_x z, 0)}{\partial(z/\delta)}\left(\frac{z}{\delta}\right) + O\left(\frac{z^2}{\delta^2}\right) \tag{3.4b}$$

for $k_x \sim O(1/z)$, and

$$h(k_x l_I, z/\delta) = h(k_x l_I, 0) + \frac{\partial h(k_x l_I, 0)}{\partial(z/\delta)}\left(\frac{z}{\delta}\right) + O\left(\frac{z^2}{\delta^2}\right) \tag{3.4c}$$

for $1/\delta \ll k_x \ll 1/z$, respectively. If the prediction (2.5) given by Perry *et al.* (1986) is correct, it is now expected that $h(k_x l_I, 0) \to A$ in the limit as $z/\delta \to 0$. Although the detailed convergence to this possible limiting behaviour would be answered only by additional measurements at higher Reynolds numbers, it is evident that in this limit, (3.1*a*), (3.1*b*) and (3.3) become identical to (2.2*b*), (2.3*b*) and (2.5) by setting

$\tilde{h}_1(k_x\delta, 0) = h_1(k_x\delta)$, $\tilde{h}_2(k_x z, 0) = h_2(k_x z)$ and $h(k_x l_I, 0) = A$. This implies that the original model of Perry *et al.* (1986) would be strictly valid in the limit as $z/\delta \to 0$. As such, the emergence of a well-developed k_x^{-1} spectrum in the sense of Perry *et al.* (1986) might be observed only for very small z/δ at extremely high Reynolds numbers, as was recently proposed by Baars & Marusic (2020*a*). Care therefore needs to be taken in interpreting (2.5) obtained from Perry *et al.* (1986) for the experimental data where z/δ is not infinitesimal but small. In fact, (3.4*c*) indicates that the wall-normal variation of the spectral intensity for $1/\delta \ll k_x \ll 1/z$ would be of $O(z/\delta)$. Since $z/\delta \sim O(10^{-1})$ in layer I, the premultiplied spectrum for $O(1/\delta) < k_x < O(1/z)$ is expected to change with z/δ at least by $O(10^{-1})$. This is exactly seen in the experimental data in figure 3 as well as in other previous papers (Morrison *et al.* 2001, 2004; Rosenberg *et al.* 2013), and it is due to the 'finite z/δ' of the measurement locations at finite Reynolds numbers.

(iii) Townsend–Perry constant: The general form of spectrum given by (3.3) suggests that in practice (at finite Reynolds number and finite z/δ), the premultiplied spectrum in the absence of a well-developed k_x^{-1} spectrum in layer I would offer little insight into the Townsend–Perry constant A (see (2.5)). This also implies that the log-linear behaviour of the streamwise turbulence intensity, previously reported to emerge in the form of (1.1) (e.g. Marusic *et al.* 2013), is not the one expected directly from the model of Perry *et al.* (1986), because the spectrum intensity varies with z/δ without necessarily exhibiting a well-developed k_x^{-1} spectrum. In this respect, it is now important to understand how the logarithmic wall-normal dependence of streamwise turbulence intensity would emerge without having a k_x^{-1} spectrum.

3.2. *Turbulence intensity*

From the discussion given above, a schematic diagram of the premultiplied power-spectral density for the model in the present study is sketched in figure 4. This schematic diagram is also consistent with the spectra observed in figure 3 (compare figure 3 with figure 4). The primary differences from the schematic diagram in figure 1 are: (1) a non-trivial form of spectrum for $1/\delta \ll k \ll 1/z$; (2) the intensity dependent on z/δ for all k_x; (3) the spectrum with order unity intensity for $k_x \in [a_I/\delta, b_I/\delta]$ from (3.1*a*) and (3.1*b*) (red-shaded region in figure 4), where a_I and b_I are $O(1)$ constants to be defined below. In this model, the spectrum for $a_I/\delta \le k_x \le b_I/z$ is set to take the following form without loss of generality:

$$\frac{k_x\,\Phi_{uu}(k_x, z)}{u_\tau^2} = h\left(k_x l_I, \frac{z}{\delta}\right) \quad \text{for } a_I/\delta \ll k_x \ll b_I/z, \tag{3.5a}$$

and a_I and b_I are given such that

$$\frac{k_x\,\Phi_{uu}(k_x, z)}{u_\tau^2} \sim O(A_{I,0}) \quad \text{for } a_I/\delta \le k_x \le b_I/z, \tag{3.5b}$$

where $A_{I,0}$ is a constant of $O(1)$, and such that $\Delta A_{I,0}(k_x l_I, z/\delta)(\equiv k_x\,\Phi(k_x, z)/u_\tau^2 - A_{I,0})$ satisfies

$$\underbrace{\int_{\ln(a_I/\delta)}^{\ln(b_I/z)} \Delta A_{I,0}\left(k_x l_I, \frac{z}{\delta}\right) \mathrm{d}(\ln k_x)}_{\equiv A_{I,1}(z/\delta)} \sim O\left(\frac{z}{\delta}\right). \tag{3.5c}$$

In other words, with the spectrum, $A_{I,0}$, a_I and b_I can be chosen such that the area below the premultiplied spectrum for $a_I/\delta \le k_x \le b_I/z$ is approximated by the red-shaded region

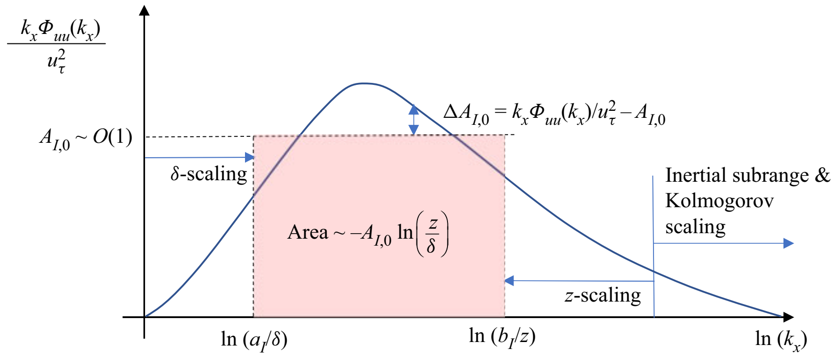

Figure 4. A schematic diagram of the proposed model in the present study for the spectra in layer I.

in figure 4 with an error of $O(z/\delta)$. We note that such a choice of $A_{I,0}$, a_I and b_I must always be possible, because the mean-value theorem for integrals ensures the existence of $A_{I,M}(z/\delta)$ satisfying

$$A_{I,M}(z/\delta) = \left[\ln\left(\frac{b_I}{z}\right) - \ln\left(\frac{a_I}{\delta}\right)\right]^{-1} \int_{\ln(a_I/\delta)}^{\ln(b_I/z)} \frac{k_x\, \Phi_{uu}(k_x, z/\delta)}{u_\tau^2}\, \mathrm{d}(\ln k_x). \tag{3.6a}$$

Here, $A_{I,M}(z/\delta)$ can further be written such that

$$A_{I,M}(z/\delta) = A_{I,0} + A_{I,1}(z/\delta), \tag{3.6b}$$

where $A_{I,1}(z/\delta)$ remains at $O(z/\delta)$ by applying the Taylor series expansion to $A_{I,M}(z/\delta)$ at any wall-normal location in layer I.

From (2.1) and (3.6), the streamwise turbulence intensity is now written as

$$\begin{aligned}\frac{\overline{u'u'}}{u_\tau^2} &= \int_{-\infty}^{\infty} \frac{k_x\, \Phi_{uu}(k_x; z)}{u_\tau^2}\, \mathrm{d}(\ln k_x) = \int_{\ln(a_I/\delta)}^{\ln(b_I/z)} \frac{k_x\, \Phi_{uu}(k_x)}{u_\tau^2}\, \mathrm{d}(\ln k_x) + C_I(z; Re_\tau) \\ &= \left[A_{I,0} + A_{I,1}\left(\frac{z}{\delta}\right)\right]\left[\ln\left(\frac{b_I}{z}\right) - \ln\left(\frac{a_I}{\delta}\right)\right] + C_I(z; Re_\tau) \\ &= -\left[A_{I,0} + A_{I,1}\left(\frac{z}{\delta}\right)\right]\ln\left(\frac{z}{\delta}\right) + B_I(z; Re_\tau),\end{aligned} \tag{3.7a}$$

where

$$C_I\,(z; Re_\tau) = \frac{\overline{u'u'}}{u_\tau^2} - \int_{\ln(b_I/\delta)}^{\ln(a_I/z)} \frac{k_x\, \Phi_{uu}(k_x)}{u_\tau^2}\, \mathrm{d}(\ln k_x), \tag{3.7b}$$

$$B_I\,(z; Re_\tau) = C_I\,(z; Re_\tau) - \left[A_{I,0} + A_{I,1}\left(\frac{z}{\delta}\right)\right]\ln\left(\frac{b_I}{a_I}\right). \tag{3.7c}$$

Here, $C_I(z; Re_\tau)$ represents the contribution of the spectrum for $k_x < a_I/\delta$ and $k_x > b_I/z$ to the turbulence intensity, and it should depend weakly on z and Re_τ due to the Kolmogorov-scaling part in figure 4 and the weak (z/δ)-dependence of (3.4a) and (3.4b) within layer I. In (3.7a) and (3.7c), the Taylor series expansion allows $A_{I,1}(z/\delta)$ to be approximated further as

$$A_{I,1}\left(\frac{z}{\delta}\right)=A_{I,1}\left(\frac{z_{I,m}}{\delta}\right)+\left.\frac{\mathrm{d}A_{I,1}}{\mathrm{d}(z/\delta)}\right|_{z=z_{I,m}}\frac{(z-z_{I,m})}{\delta}+O\left(\frac{|z-z_{I,m}|^2}{\delta^2}\right), \tag{3.8}$$

where $z_{I,m}=\sqrt{z_m z_o}$ is chosen to be the geometric mean of z_m and z_o, so that the right-hand side of (3.8) becomes a good approximation to $A_{I,1}$ over the entire layer I in the 'logarithmic' wall-normal coordinate. The same approximation can be applied to $C_I(z;Re_\tau)$ in (3.7*b*). Since $z_{I,m}/\delta$ is a function of Re_τ from $z_m/\delta=3.6Re_\tau^{-0.5}$, the streamwise turbulence intensity is finally given by

$$\frac{\overline{u'u'}}{u_\tau^2}=-A_I(Re_\tau)\ln\left(\frac{z}{\delta}\right)+B_I(z_{I,m};Re_\tau)+O\left(\frac{z}{\delta}\right), \tag{3.9}$$

where $A_I(Re_\tau)=A_{I,0}+A_{I,1}(z_{I,m}/\delta)$ and the error at $O(z/\delta)$ stems from approximation of $C_I(z;Re_\tau)$ in (3.7*c*) for layer I. We also note that in layer I, the Reynolds shear stress would evidently be $-\overline{u'w'}/u_\tau^2=\text{const}+O(z/\delta)$, where w' is the wall-normal velocity fluctuation. Therefore (3.9) is consistent with the original attached eddy model of Townsend (1976) with an error of $O(z/\delta)$.

Now, the logarithmic wall-normal dependence of the streamwise turbulence intensity is retrieved in (3.9) as in the classical theories (Townsend 1976; Perry & Chong 1982; Perry *et al.* 1986) with a small error at $O(z/\delta)\sim 10^{-1}$, indicating that the classical result is indeed a reliable first approximation to the streamwise turbulence intensity in layer I. Importantly, the Townsend–Perry constant A_I in this case emerges as a function of Re_τ, and, to our knowledge, the present study provides the first rigorous derivation for this feature – it would depend weakly on Re_τ, given $A_{I,1}\sim O(z/\delta)$ from (3.6*b*). We note that this is a combined consequence of (3.6*b*) and the nature of z_m (or $z_{I,m}$) depending on Re_τ. Since z_m is a function of Re_τ due to the viscous wall effect, the Reynolds-number-dependent nature of $A_I(Re_\tau)$ in (3.9) essentially originates from the role of viscosity ignored in the original theories (e.g. Townsend 1976; Perry & Chong 1982; Perry *et al.* 1986). This is evident from $z_m/\delta\to 0$ in the limit as $Re_\tau\to\infty$: that is, the velocity slip condition (i.e. non-zero spectrum at $z=z_m$) reaches all the way down to the wall in such a limit. In this case, as $z/\delta\to 0$, A_I becomes constant from (3.6*b*), and the error of $O(z/\delta)$ in (3.9) vanishes. Therefore (3.9) consequently becomes identical to (2.6) from the original model of Perry *et al.* (1986) in the limit as $Re_\tau\to\infty$ and $z/\delta\to 0$.

It should, however, be mentioned that the use of the mean-value theorem in (3.6) for the derivation of (3.9) is the key difference from that of (2.6) in Perry *et al.* (1986). The derivation here is more general and inclusive than that in Perry *et al.* (1986), because it does not rely on the existence of a k_x^{-1} spectrum. Instead, it suggests that a more general condition for the existence of an approximate logarithmic wall-normal dependence of the streamwise turbulence intensity is the existence of the premultiplied power-spectral density of $O(1)$ for $O(1/\delta)\le k_x\le O(1/z)$ (red-shaded region in figure 4), which is entirely consistent with the experimental data in figure 3. Here, it is important to note that this behaviour essentially originates from the spectrum scalings in (3.1*a*) and (3.1*b*), the general versions of (2.2) and (2.3) for finite z/δ, because (3.9) is simply a consequence of applying the mean-value theorem in (3.6) with them. Since (2.2) and (2.3) depict the δ-scaling inactive motions of large eddies and the z-scaling self-similar eddies, the theoretical development here is also well within the framework of the attached eddy hypothesis. Lastly, it is worth mentioning that a more accurate description for $\Delta A_{I,0}(z_{I,m}/\delta)$ may well be possible from a viewpoint of scaling with Re_τ. The recent effort made by Vassilicos *et al.* (2015) can be interpreted in such a context, as it is based on a prescribed semi-empirical description for the spectrum lying between the wavenumber ranges for (2.2*b*) and (2.5).

3.3. *Determination of A_I and B_I from experimental data*

While the analysis in §§ 3.1 and 3.2 provides an insight into the relationship between the power-spectral density and the streamwise turbulence intensity at finite Reynolds numbers, there is a practical issue in applying it to the data obtained from laboratory experiments and numerical simulations. This issue is related to how one would choose $A_{I,0}$, a_I and b_I robustly. To this end, here we propose a simple semi-empirical modelling framework for the streamwise turbulence intensity by leveraging the mean-value theorem (3.6). We start by writing the turbulence intensity as

$$\begin{aligned}\frac{\overline{u'u'}}{u_\tau^2} &= \int_{-\infty}^{\infty} \frac{k_x\,\varPhi_{uu}(z;k_x;Re_\tau)}{u_\tau^2}\,\mathrm{d}(\ln k_x)\\ &= \left[\ln\left(\frac{b_{I,s}}{z}\right) - \ln\left(\frac{a_{I,s}}{\delta}\right)\right]\varPi_I(z;Re_\tau)\\ &= \left[\ln\left(\frac{b_{I,s}}{a_{I,s}}\right) - \ln\left(\frac{z}{\delta}\right)\right]\varPi_I(z;Re_\tau),\end{aligned} \tag{3.10a}$$

where

$$\varPi_I(z;Re_\tau) = \left[\ln\left(\frac{b_{I,s}}{a_{I,s}}\right) - \ln\left(\frac{z}{\delta}\right)\right]^{-1} \int_0^{\infty} \frac{k_x\varPhi_{uu}}{u_\tau^2}\,\mathrm{d}(\ln k_x). \tag{3.10b}$$

Here, $a_{I,s}$ and $b_{I,s}$ are constants that play roles similar to those of a_I and b_I in figure 4, but their values are not necessarily the same. However, given the analysis in § 3.2, they need to be chosen from the wavenumbers of δ- and z-scaling regions of the premultiplied spectra, and have to be constant at all Reynolds numbers. While this sets out a condition for $a_{I,s}$ and $b_{I,s}$ to be met, it is also important to note that they cannot be chosen arbitrarily. Although (3.10) is supposed to automatically yield a streamwise turbulence intensity in the form of (3.7*a*) for any values of $a_{I,s}$ and $b_{I,s}$, the last line of (3.10*a*) implies that it has a single degree of freedom for the determination of A_I and B_I in (3.7*a*) (i.e. the value of $b_{I,s}/a_{I,s}$). Indeed, if $b_{I,s}/a_{I,s} < 1$ is chosen, then B_I in (3.7*a*) becomes negative from (3.10*a*), which would obviously be non-physical. Therefore the last condition for $a_{I,s}$ and $b_{I,s}$ to be met is that they must be chosen such that $\ln(b_{I,s}/a_{I,s})\,\varPi_I(z;Re_\tau)$ would represent B_I in (3.7*a*) well, while ensuring $b_{I,s}/a_{I,s} > 1$.

In the present study, $a_{I,s} = \pi/5$ and $b_{I,s} = 2\pi$ are chosen so that $\lambda_{x,I\,a}(\equiv 2\pi\delta/a_{I,s}) = 10\delta$ and $\lambda_{x,I\,b}(\equiv 2\pi z/b_{I,s}) = z$. These values are obtained by trial and error. To do so, a range of candidate values of $a_{I,s}$ and $b_{I,s}$ are first selected from the spectra in figure 3, so that $\lambda_{x,I\,a}$ and $\lambda_{x,I\,b}$ lie in the δ- and z-scaling regions, respectively. Indeed, figure 3 shows that the premultiplied spectra in layer I scale well with δ for $\lambda_x \simeq \lambda_{x,I\,a}$, and with z for $\lambda_x \simeq \lambda_{x,I\,b}$, and that $b_{I,s}/a_{I,s} > 1$, consistent with the purpose of $a_{I,s}$ and $b_{I,s}$ introduced here. Once this is ensured, the final values of $a_{I,s}$ and $b_{I,s}$ are determined by monitoring the form of $\varPi_I(z)$ within the layer. If a set of sensible values is chosen, then $\varPi_I(z)$ must exhibit a plateau around $z = z_{I,m}$ in layer I. Indeed, figure 5 demonstrates that, for the given $a_{I,s}$ and $b_{I,s}$, $\varPi_I(z)$ remains approximately constant in layer I. Once $a_{I,s}$ and $b_{I,s}$ are determined, the resulting streamwise turbulence intensity is approximated around $z = z_{I,m}$

https://doi.org/10.1017/jfm.2021.1057 Published online by Cambridge University Press

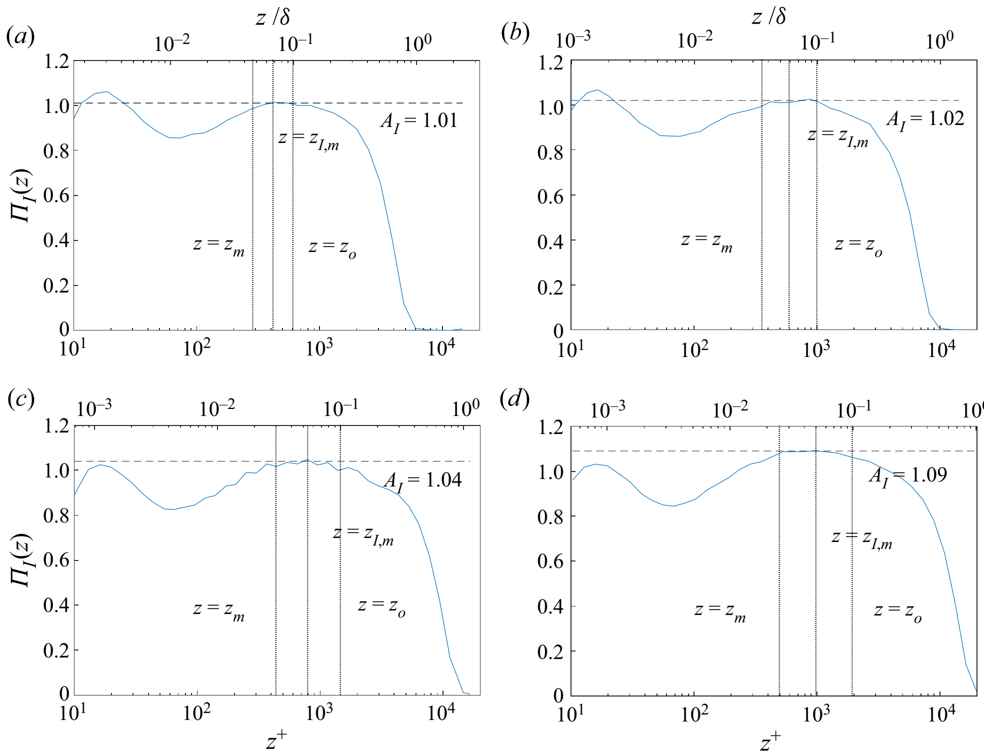

Figure 5. $\Pi_I(z)$ (solid line) from (3.10*b*), and A_I (dashed line) from (3.11*b*): (*a*) $Re_\tau = 6123$; (*b*) $Re_\tau = 10\,100$; (*c*) $Re_\tau = 14\,680$; (*d*) $Re_\tau = 19\,680$. Here, $a_{I,s} = 2\pi$ ($\lambda_{x,I\,a} = 10$) and $b_{I,s} = \pi/5$ ($\lambda_{x,I\,b} = 1$).

(see also (3.9)):

$$\frac{\overline{u'u'}}{u_\tau^2} \simeq -A_I(Re_\tau)\ln\left(\frac{z}{\delta}\right) + B_I(Re_\tau), \tag{3.11a}$$

where

$$A_I(Re_\tau) = \Pi_I(z_{I,m}; Re_\tau), \tag{3.11b}$$

$$B_I(Re_\tau) = \Pi_I(z_{I,m}; Re_\tau)\ln\left(\frac{b_{I,s}}{a_{I,s}}\right). \tag{3.11c}$$

The values of $A_I(Re_\tau)$ and $B_I(Re_\tau)$ are then obtained from (3.11*b*) and (3.11*c*), respectively. In the present study, the values of $a_{I,s} = \pi/5$ and $b_{I,s} = 2\pi$ are first determined at $Re_\tau = 19\,680$ and are subsequently used for the other Reynolds numbers. Figure 6 shows the streamwise turbulence intensity and its approximation from (3.11). With the given $a_{I,s}$ and $b_{I,s}$, the proposed framework in (3.10) determines both A_I and B_I well, so that (3.11*a*) becomes a good fit to the turbulence intensity in layer I at all the Reynolds numbers. The computed values of $A_I(Re_\tau)$ and $B_I(Re_\tau)$ are also reported in table 1 with the approximation error of the model (3.11*a*) in layer I. The maximum error is found to be less than about 4 % at all the Reynolds numbers considered.

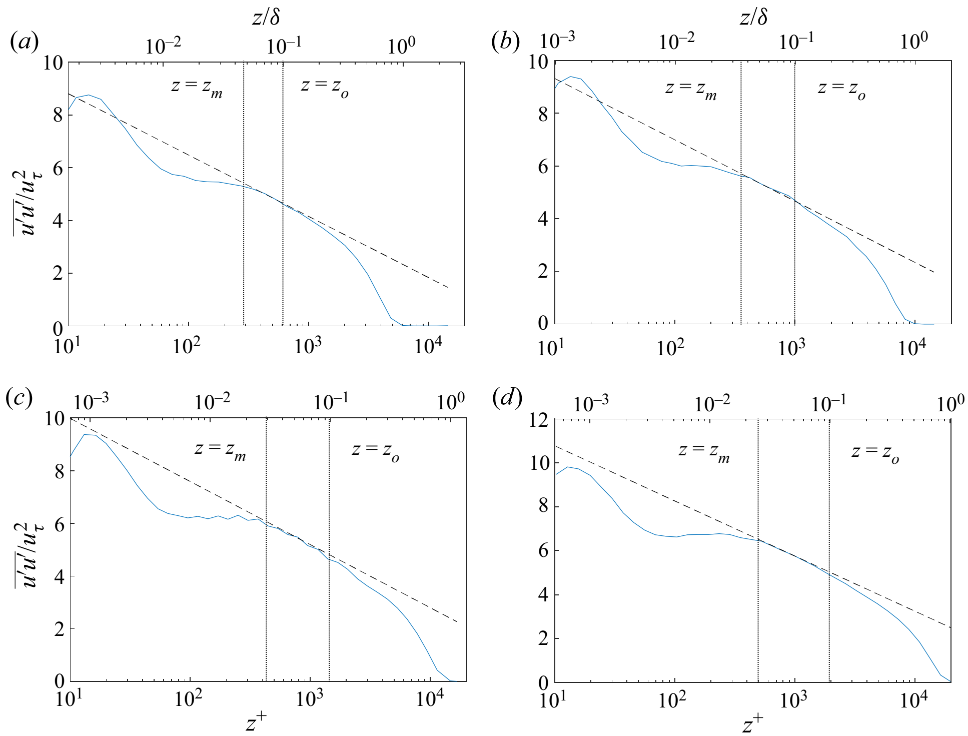

Figure 6. Streamwise turbulence intensity (solid line) and its approximation given by (3.11) (dashed line) in layer I: (*a*) $Re_\tau = 6123$; (*b*) $Re_\tau = 10\,100$; (*c*) $Re_\tau = 14\,680$; (*d*) $Re_\tau = 19\,680$. Here, $a_{I,s} = \pi/5$ ($\lambda_{x,I\,a}/\delta = 10$) and $b_{I,s} = 2\pi$ ($\lambda_{x,I\,b}/z = 1$).

Re_τ	6123	10 100	14 680	19 680
A_I	1.01	1.02	1.04	1.09
B_I	2.33	2.35	2.39	2.51
Error	1.1 %	1.6 %	4.1 %	2.5 %

Table 1. The Reynolds-number dependence of A_I and B_I from (3.11) with $a_{I,s} = \pi/5$ ($\lambda_{x,I\,a}/\delta = 10$) and $b_{I,s} = 2\pi$ ($\lambda_{x,I\,b}/z = 1$). Here, Error $\equiv \max_z |\overline{u'u'}_{model} - \overline{u'u'}|/\overline{u'u'}$ for $z \in [z_m, z_o]$, where $\overline{u'u'}_{model}$ is from (3.11), and it indicates the maximum error of the proposed model in layer I.

4. Extension to layer II

4.1. *Scaling of spectra*

The model developed in § 3 is further extended to layer II where $z_i \leq z \leq z_m$ with $z_i^+ = 200$ and $z_m^+ = 3.6Re_\tau^{1/2}$ ($z_m^+ = 505$ at $Re_\tau = 19\,680$). In particular, here we shall take an empirical approach for the information that cannot be retrieved solely with scaling arguments. Given the importance of viscous forces in this layer, the power-spectral density should be a function of u_τ, k_x, z, δ and $\delta_\nu (\equiv \nu/u_\tau)$. Without loss of generality, the outer-scaling part of the spectrum for $k_x \sim O(1/\delta)$ would therefore be written as a function of z^+ and $Re_\tau (= \delta/\delta_\nu)$ as

$$\frac{\Phi_{uu}(k_x\delta, z^+, Re_\tau)}{u_\tau^2} = \frac{\Phi_{uu}(k_x, z^+, Re_\tau)}{\delta u_\tau^2} = g_{1,II}(k_x\delta, z^+, Re_\tau), \tag{4.1a}$$

with the corresponding premultiplied spectrum

$$\frac{k_x\,\Phi_{uu}(k_x)}{u_\tau^2} = k_x\delta\, g_{1,II}(k_x\delta, z^+, Re_\tau) = h_{1,II}(k_x\delta, z^+, Re_\tau). \tag{4.1b}$$

Similarly, the z-scaling part of the spectrum is written as

$$\frac{\Phi_{uu}(k_x z, z^+, Re_\tau)}{u_\tau^2} = \frac{\Phi_{uu}(k_x, z^+, Re_\tau)}{z u_\tau^2} = g_{2,II}(k_x z, z^+, Re_\tau), \tag{4.2a}$$

and the premultiplied spectrum is

$$\frac{k_x\,\Phi_{uu}(k_x)}{u_\tau^2} = k_x z\, g_{2,II}(k_x z, z^+, Re_\tau) = h_{2,II}(k_x z, z^+, Re_\tau). \tag{4.2b}$$

Here, we note that the introduction of a possible dependence on z^+ and Re_τ in (4.1) and (4.2) is to describe the viscous wall effect on z- and δ-scaling motions, the scaling and the corresponding energy balance of which were discussed in detail in Hwang (2016) and Cho *et al.* (2018) using a linear theory and numerical simulation data. While the contribution of δ-scaling motions is sometimes accounted for separately (Baars & Marusic 2020*a*,*b*; Deshpande *et al.* 2020), here we shall consider the contributions of all the energy-containing motions simultaneously.

The spectra given in (4.1) and (4.2) suggest that the dependence of $h_{1,II}$ and $h_{2,II}$ on z^+ and Re_τ would be the major complication in extending the analysis in § 3 to layer II. Therefore, from here, we shall further proceed by empirically modelling the experimental data of Samie *et al.* (2018) in layer II. As discussed in § 2, the contour lines for $\lambda_x \gtrsim 10\delta$ in figure 2 are not parallel to $\lambda_x = 10\delta$. They rather appear to fall off approximately linearly towards the wall in the logarithmic coordinates, indicating that the outer-scaling part of the spectra would empirically follow a mixed scale of $\lambda_x/\delta \sim (z^+)^p$, where p is a positive number to be determined. Based on this observation, (4.1) may be written as

$$h_{1,II}(k_x\delta, z^+, Re_\tau) \simeq \tilde{h}_{1,II}\left(k_x\delta_{II}, \frac{z}{\delta_{II}}\right), \tag{4.3a}$$

where $\delta_{II} = \delta(z^+)^p$ is the empirical similarity length scale formed by δ and z^+, and the z/δ_{II}-dependence is introduced to admit the small deviation of the spectra in layer II similarly to the case in layer I (§ 3.1). As for the inner-scaling part of the spectra, the contour lines for $10^{-2}\delta \leq \lambda_x \leq 10^{-1}\delta$ in layer II (figure 2) are still approximately parallel to $\lambda_x = z$. Therefore $h_{2,II}(k_x z, z^+)$ in (4.2) is also written as

$$h_{2,II}(k_x z, z^+, Re_\tau) \simeq \tilde{h}_{2,II}\left(k_x z, \frac{z}{\delta_{II}}\right), \tag{4.3b}$$

where z/δ_{II} is introduced to allow for a small variation in the wall-normal location. Figure 7 confirms that the empirical scalings in (4.3*a*) and (4.3*b*) are reasonably good: the outer-scale part of the premultiplied spectra scales well with δ_{II} for $p = 0.41$ obtained empirically (figure 7*a*), while the inner-scaling part shows good scaling with z (figure 7*b*).

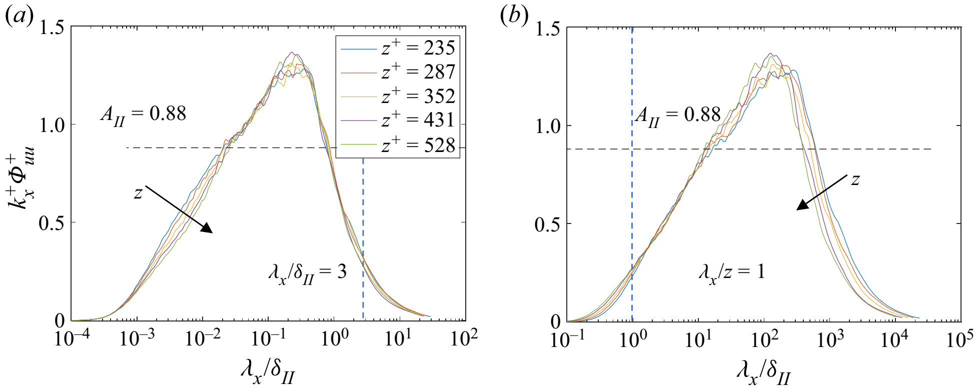

Figure 7. Premultiplied streamwise power-spectral density of streamwise velocity in layer II ($Re_\tau = 19\,680$): (*a*) δ_{II}-scaling and (*b*) z-scaling. Here, $\delta_{II} = \delta(z^+)^p$ with $p = 0.41$.

The form of (4.3*a*) and (4.3*b*) is now identical to that of (3.1*a*) and (3.1*b*), if δ is replaced by δ_{II}. The procedure in § 3.1 can therefore be applied exactly in the same manner. Without loss of generality, this yields

$$\frac{k_x\,\Phi_{uu}(k_x)}{u_\tau^2} = h_{II}\left(k_x l_{II}, \frac{z}{\delta_{II}}\right) \tag{4.4}$$

for $1/\delta_{II} \ll k_x \ll 1/z$ with $z \ll l_{II} \ll \delta_{II}$, and the resulting premultiplied power-spectral density for $1/\delta_{II} \ll k_x \ll 1/z$ is given by

$$\frac{\Phi_{uu}(k_x)}{u_\tau^2} = \frac{h_{II}(k_x l_{II}, z/\delta_{II})}{k_x}. \tag{4.5}$$

Equation (4.5) suggests that a k_x^{-1} spectrum would also be observed at each wall-normal location in layer II. As shown in figure 7, such a spectrum does seem to appear for $50z \lesssim \lambda_x \lesssim 0.5\delta_{II}$ in the form of a peak or a narrow plateau. It also indicates that the intensity of the k_x^{-1} spectrum would vary in the wall-normal direction by $O(z/\delta_{II})$ in layer II. Given the definition of layer II, $z/\delta_{II} \sim O(10^{-2})$. Figure 7 shows that the variation of the peak intensity of each premultiplied spectrum is much smaller than that in layer I (compare with figure 3), supporting the relevance of (4.5).

4.2. *Turbulence intensity*

Given the form of spectra shown in (4.3*a*), (4.3*b*) and (4.5), the turbulence intensity in layer II can also be obtained by applying the same procedure in § 3.2. In Appendix A, it is shown that the streamwise turbulence intensity in layer II takes the following form:

$$\frac{\overline{u'u'}}{u_\tau^2} \simeq -A_{II}(z_{II,m}; Re_\tau)\left[\ln\left(\frac{z}{\delta}\right) - p\ln(z^+)\right] + B_{II}(z_{II,m}; Re_\tau), \tag{4.6}$$

where $z_{II,m} = \sqrt{z_i z_m}$, $A_{II}(z_{II,m}; Re_\tau)$ and $B_{II}(z_{II,m}; Re_\tau)$ are defined in Appendix A. Here, we note that the term with z^+ now emerges, and it incorporates the effect of the viscosity into the original attached eddy model. Also, similarly to layer I, A_{II} and B_{II} in (4.6) are expected to depend weakly on Re_τ (see Appendix A). Lastly, following the modelling

https://doi.org/10.1017/jfm.2021.1057 Published online by Cambridge University Press

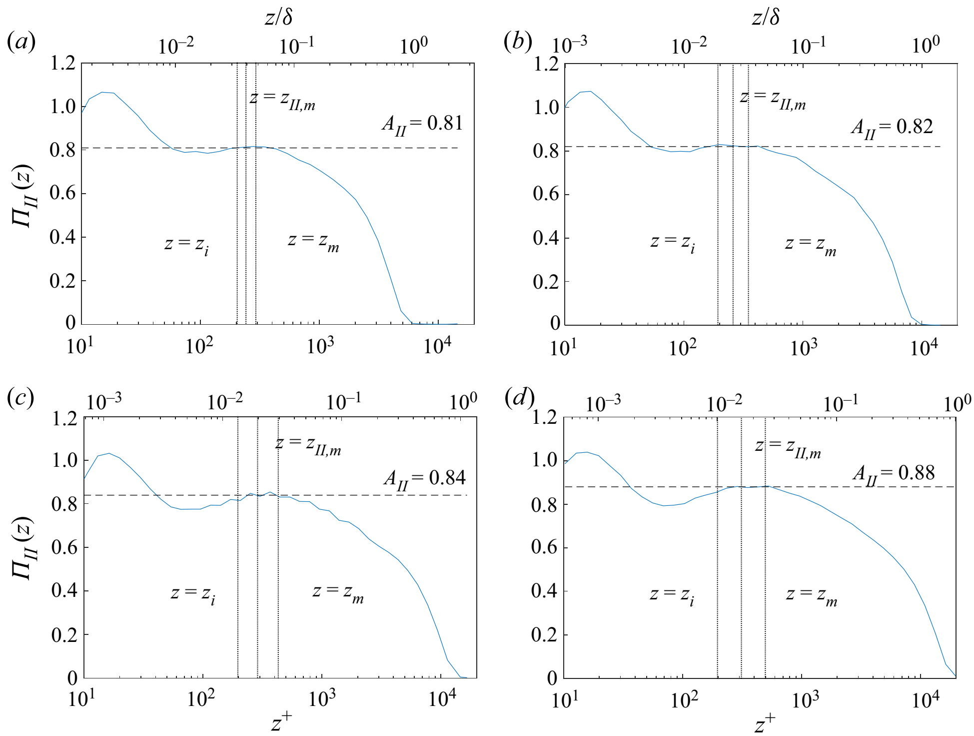

Figure 8. $\Pi_{II}(z)$ (solid line) from (4.7c) and A_{II} (dashed line) from (4.7a): (a) $Re_\tau = 6123$; (b) $Re_\tau = 10\,100$; (c) $Re_\tau = 14\,680$; (d) $Re_\tau = 19\,680$. Here, $a_{II,s} = 2\pi/3$ ($\lambda_{x,II\,a}/\delta_{II} = 3$) and $b_{II,s} = 2\pi$ ($\lambda_{x,II\,b}/z = 1$).

procedure for layer I in § 3.3, $A_{II}(z_{II,m}; Re_\tau)$ and $B_{II}(z_{II,m}; Re_\tau)$ can be semi-empirically determined, such that

$$A_{II}(Re_\tau) = \Pi_{II}(z_{II,m}; Re_\tau), \tag{4.7a}$$

$$B_{II}(Re_\tau) = \Pi_{II}(z_{II,m}; Re_\tau) \ln\left(\frac{b_{II,s}}{a_{II,s}}\right), \tag{4.7b}$$

where

$$\Pi_{II}(z; Re_\tau) = \left[\ln\left(\frac{b_{II,s}}{z}\right) - \ln\left(\frac{a_{II,s}}{\delta_{II}}\right)\right]^{-1} \int_0^\infty \frac{k_x \Phi_{uu}}{u_\tau^2}\, \mathrm{d}(\ln k_x), \tag{4.7c}$$

and $a_{II,s}$ and $b_{II,s}$ are the fitting constants for the model in (4.6), similarly to $a_{I,s}$ and $b_{I,s}$ in § 3.3. In the present study, $a_{II,s} = 2\pi/3$ and $b_{II,s} = 2\pi$ are obtained by trial and error with the experimental data for all the Reynolds numbers. The determination procedure of $a_{II,s} = 2\pi/3$ and $b_{II,s} = 2\pi$ follows that in § 3.3 exactly. This leads to $\lambda_{x,II\,a}(\equiv 2\pi\delta_{II}/a_{II,s}) = 3\delta_{II}$ and $\lambda_{x,I\,b}(\equiv 2\pi z/b_{II,s}) = z$. We note that the premultiplied spectra in layer II scale well with δ_{II} for $\lambda_x \simeq \lambda_{x,II\,a}$ (figure 7a) and with z for $\lambda_x \simeq \lambda_{x,II\,b}$ (figure 7b), serving the introduced purpose of $a_{II,s}$ and $b_{II,s}$. Figure 8 shows $\Pi_{II}(z)$ and the corresponding $A_{II}(Re_\tau)$ determined at all the Reynolds numbers. Similar to the case of layer I, $\Pi_{II}(z)$ remains approximately constant in layer II with the given $a_{II,s}$ and $b_{II,s}$, and the resulting $A_{II}(Re_\tau)$ is also found to depend weakly on the Reynolds number. The streamwise turbulence intensity and its approximation from (3.11) are shown in figure 9. For the given $a_{II,s}$ and $b_{II,s}$, the model in (4.6) and (4.7) well approximates the streamwise

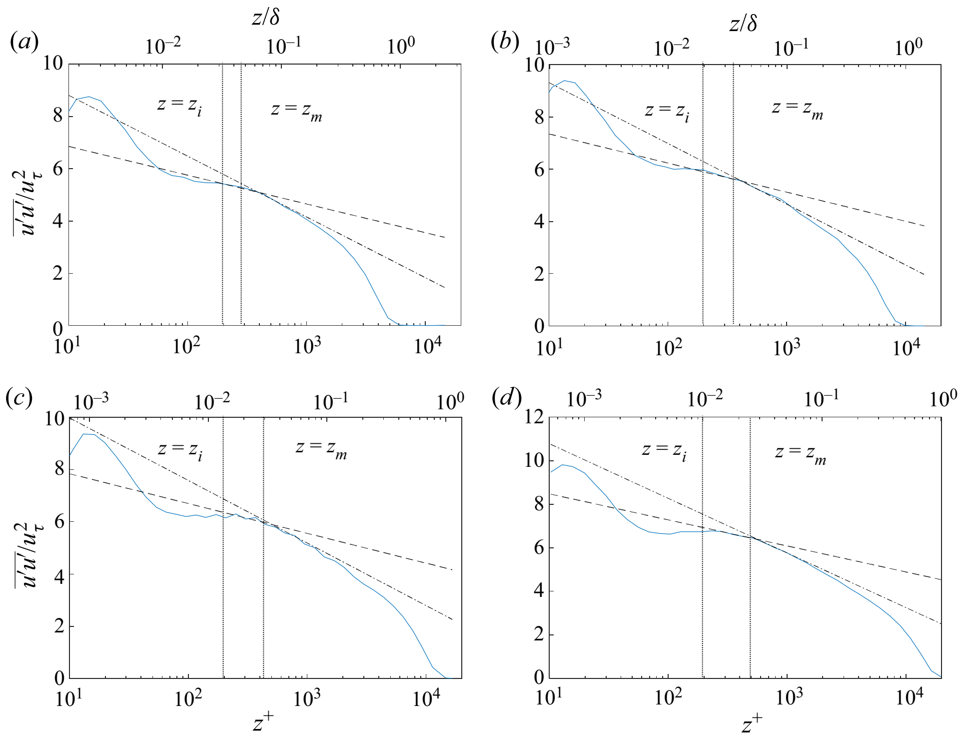

Figure 9. Streamwise turbulence intensity (solid line) and its approximation given by (4.6) (dashed line) in layer II: (*a*) $Re_\tau = 6123$; (*b*) $Re_\tau = 10\,100$; (*c*) $Re_\tau = 14\,680$; (*d*) $Re_\tau = 19\,680$. Here, $a_{II,s} = 2\pi/3$ ($\lambda_{x,II\,a}/\delta_{II} = 3$) and $b_{II,s} = 2\pi$ ($\lambda_{x,II\,b}/z = 1$). The streamwise turbulence intensity from model (3.11*a*) for layer I (dashed-dotted line) is also plotted for comparison.

Re_τ	6123	10 100	14 680	19 680
A_{II}	0.81	0.82	0.84	0.88
B_{II}	0.89	0.90	0.92	0.97
Error	0.8 %	1.1 %	3.0 %	0.8 %

Table 2. The Reynolds-number dependence of A_{II} and B_{II} from (4.7) with $a_{II,s} = 2\pi/3$ and $b_{II,s} = 2\pi$. Here, Error $= \max_z |\overline{u'u'}_{model} - \overline{u'u'}|/\overline{u'u'}$ for $z \in [z_i, z_m]$, where $\overline{u'u'}_{model}$ is from (4.6), and it indicates the maximum error of the proposed model in layer II.

turbulence intensity in layer II at all the Reynolds numbers. Finally, the values of $A_{II}(Re_\tau)$ and $B_{II}(Re_\tau)$ are listed in table 2. The maximum error of the model of (4.6) remains at less than 3 %.

5. Conclusions

In the present study, we have presented a spectrum-based attached model by generalising that of Perry *et al.* (1986) for small but finite z/δ and for finite Reynolds numbers. In layer I (the upper logarithmic layer or inertial sublayer), the analysis showed that, without loss of generality, the intensity of the spectra should vary in the wall-normal direction considerably, consistent with the experimental data. By applying the mean-value theorem to spectra in layer I, the streamwise turbulence intensity is subsequently calculated. This revealed that the Townsend–Perry constant must be weakly dependent on Reynolds number. More importantly, it was shown that a more general condition for the approximate logarithmic wall-normal dependence of the turbulence intensity is the existence of premultiplied power-spectral intensity of $O(1)$ for $1/\delta \lesssim k_x \lesssim 1/z$, and that the emergence of k_x^{-1} spectra is not a necessary condition for such a form of turbulence intensity. The analysis was further extended to layer II (the lower logarithmic layer or mesolayer), and a near-wall correction term for the turbulence intensity in this layer was subsequently proposed. Finally, the predictions of the proposed model and all the related assumptions have been carefully validated with the high-fidelity experimental data by Samie *et al.* (2018).

Perhaps the primary contribution of the present study would lie in addressing the two issues questioned repeatedly for a long time: (1) Would a k_x^{-1} spectrum be necessary for the logarithmic wall-normal dependence of turbulence intensity? (2) Is the early observation of Morrison *et al.* (2001, 2004), referred to as the 'incomplete similarity', inconsistent with the model of Perry *et al.* (1986)? The present study showed that the answer to the first question is 'no', because the more general condition is the existence of premultiplied power-spectral intensity of $O(1)$ for $1/\delta \lesssim k_x \lesssim 1/z$. We note that this condition is also physically consistent with the notion of the attached eddy hypothesis of Townsend (1976) (see the discussion in § 3.2) and is therefore inclusive of the original model of Perry *et al.* (1986). The answer to the second question is that the discrepancy between the theoretical result of Perry *et al.* (1986) and the observation of Morrison *et al.* (2001, 2004) originates from the size of z/δ in the 'idealised theoretical model' and the 'practical experimental measurement': the former assumes $z/\delta \ll 1$, which strictly implies z in the limit as $z/\delta \to 0$, whereas the latter considers small but still finite z/δ for a 'practical' reason and/or due to the 'conventional' definition of the logarithmic layer. Indeed, if the assumption $z/\delta \to 0$ is relaxed, then the theoretical model does exhibit a behaviour consistent with the experimental data.

Finally, the model proposed in this study may well be refined further by making additional modelling efforts. Such tasks include semi-empirical description of the turbulence intensity above layer I and below layer II. The Kolmogorov-scaling part of the spectrum in figure 4 can also be modelled in a more delicate manner like in the original model of Perry *et al.* (1986). These tasks remain for future work.

Acknowledgements. We are grateful to anonymous referees who contributed to improvement of § 3.1. We are also grateful to Professor E.J. Hinch, who shared a helpful discussion on (3.2).

Funding. Y.H. gratefully acknowledges the financial support from the Engineering and Physical Science Research Council (EPSRC; EP/T009365/1) in the UK, the Leverhulme trust (RPG-2019-123) and the University of Melbourne through a visiting fellowship. N.H. and I.M. gratefully acknowledge helpful discussions with R. Deshpande and the financial support of the Australian Research Council.

Declaration of interests. The authors report no conflict of interest.

Author ORCIDs.
Yongyun Hwang https://orcid.org/0000-0001-8814-0822;
Ivan Marusic https://orcid.org/0000-0003-2700-8435.

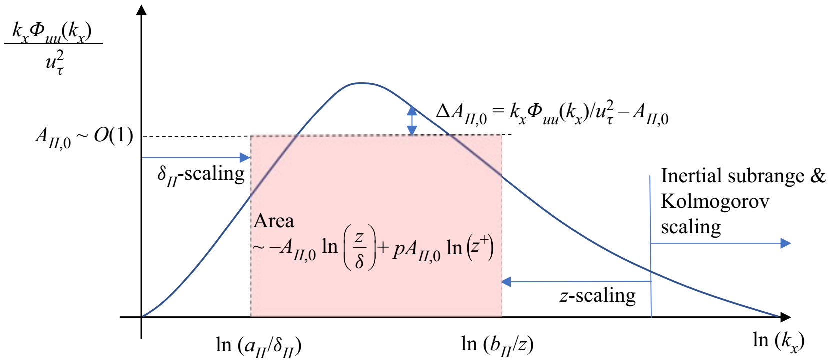

Figure 10. A schematic diagram of the proposed model for the spectra in layer II.

Appendix A. Streamwise turbulence intensity in layer II

Similarly to the model for layer I in § 3.1 (figure 4), a schematic diagram of the spectrum in layer II can be sketched as shown in figure 10. Given the discussion in § 4.1, the spectrum for $a_{II}/\delta_{II} \leq k_x \leq b_{II}/z$ in layer II takes the form

$$\frac{k_x\,\Phi_{uu}(k_x)}{u_\tau^2} = h_{II}\left(k_x l_{II}, \frac{z}{\delta_{II}}\right) \quad \text{for } a_{II}/\delta_{II} \ll k_x \ll b_{II}/z, \tag{A1a}$$

and a_{II} and b_{II} are given such that

$$\frac{k_x\,\Phi_{uu}(k_x)}{u_\tau^2} \sim O(A_{II,0}) \quad \text{at } k_x = a_{II}/\delta_{II} \text{ and } k_x = b_{II}/z, \tag{A1b}$$

where $A_{II,0}$ is a constant of $O(1)$, and such that $\Delta A_{II,0}(k_x)(\equiv k_x\Phi(k_x)/u_\tau^2 - A_{II,0})$ satisfies

$$\underbrace{\int_{\ln(a_{II}/\delta_{II})}^{\ln(b_{II}/z)} \Delta A_{II,0}(k_x)\,\mathrm{d}(\ln k_x)}_{\equiv A_{II,1}(z/\delta_{II})} \sim O\left(\frac{z}{\delta_{II}}\right). \tag{A1c}$$

Like the analysis in § 3, $A_{II,0}$, a_{II} and b_{II} here are chosen such that the area below the premultiplied spectrum for $a_{II}/\delta \leq k_x \leq b_{II}/z$ is approximated by the red-shaded region in figure 10 with an error of $O(z/\delta_{II})$. Such a choice of $A_{II,0}$, a_{II} and b_{II} must always be possible, because the mean-value theorem ensures the existence of $A_{II,M}(z/\delta)$ such that

$$A_{II,M}(z/\delta_{II}) = \left[\ln\left(\frac{b_{II}}{z}\right) - \ln\left(\frac{a_{II}}{\delta_{II}}\right)\right]^{-1} \int_{\ln(a_{II}/\delta_{II})}^{\ln(b_{II}/z)} \frac{k_x\,\Phi_{uu}(k_x;\, z/\delta)}{u_\tau^2}\,\mathrm{d}(\ln k_x), \tag{A2a}$$

where

$$A_{II,M}(z/\delta_{II}) = A_{II,0} + A_{II,1}(z/\delta_{II}), \tag{A2b}$$

with $A_{II,1}(z/\delta_{II})$ being of $O(z/\delta_{II})$ from the Taylor expansion of $A_{II,M}(z/\delta_{II})$.

https://doi.org/10.1017/jfm.2021.1057 Published online by Cambridge University Press

The turbulence intensity is subsequently written as

$$\begin{aligned}\frac{\overline{u'u'}}{u_\tau^2} &= \int_{-\infty}^{\infty} \frac{k_x\,\Phi_{uu}(k_x;z)}{u_\tau^2}\,\mathrm{d}(\ln k_x) = \int_{\ln(a_{II}/\delta_{II})}^{\ln(b_{II}/z)} \frac{k_x\,\Phi_{uu}(k_x)}{u_\tau^2}\,\mathrm{d}(\ln k_x) + C_{II}(z;Re_\tau)\\ &= \int_{\ln(b_{II}/\delta_{II})}^{\ln(a_{II}/z)} A_{II,0}\,\mathrm{d}(\ln k_x) + \int_{\ln(a_{II}/\delta_{II})}^{\ln(b_{II}/z)} \Delta A_{II,0}(z/\delta_{II})\,\mathrm{d}(\ln k_x) + C_{II}(z;Re_\tau)\\ &= -\left[A_{II,0} + A_{II,1}\left(\frac{z}{\delta_{II}}\right)\right]\ln\left(\frac{z}{\delta_{II}}\right) + B_{II}(z;Re_\tau),\end{aligned} \tag{A3a}$$

where

$$C_{II}(z;Re_\tau) = \frac{\overline{u'u'}}{u_\tau^2} - \int_{\ln(a_{II}/\delta_{II})}^{\ln(b_{II}/z)} \frac{k_x\,\Phi_{uu}(k_x)}{u_\tau^2}\,\mathrm{d}(\ln k_x), \tag{A3b}$$

$$B_{II}(z;Re_\tau) = C_{II}(z;Re_\tau) + \left[A_{II,0} + A_{II,1}\left(\frac{z}{\delta_{II}}\right)\right]\ln\left(\frac{b_{II}}{a_{II}}\right). \tag{A3c}$$

Here, $C_{II}(z;Re_\tau)$ represents the contribution of the spectrum for $k_x < a_{II}/\delta$ and $k_x > b_{II}/z$ to the turbulence intensity, and it would depend weakly on z and Re_τ due to the Kolmogorov-scaling part in figure 10. The turbulence intensity is further approximated as

$$\frac{\overline{u'u'}}{u_\tau^2} = -A_{II}(Re_\tau)\left[\ln\left(\frac{z}{\delta}\right) - p\ln z^+\right] + B_{II}(z_{II,m};Re_\tau) + O\left(\frac{z}{\delta_{II}}\right), \tag{A4}$$

where $z_{II,m} = \sqrt{z_i z_m}$ and $A_{II}(Re_\tau) = A_{II,0} + A_{II,1}(z_{II,m}/\delta)$. Here, the approximation error of (A4) is estimated to be of $O(z/\delta_{II})$. This is $O(10^{-2})$ at $Re_\tau = 19\,680$ from the definition of layer II. However, it should be mentioned that, in practice, the approximation error of (A4) for the experimental data is expected to be considerably bigger than this, because (A4) also depends on the accuracy of the empirical relations in (4.3a) and (4.3b).

References

Afzal, N. 1976 Millikan's argument at moderately large Reynolds number. *Phys. Fluids* **19**, 600–602.

Afzal, N. 1982 Fully developed turbulent flow in a pipe: an intermediate layer. *Ing.-Arch.* **52**, 355–377.

Afzal, N. & Yajnik, K. 1973 Analysis of turbulent pipe and channel flows at moderately large Reynolds number. *J. Fluid Mech.* **61**, 23–31.

del Álamo, J.C. & Jiménez, J. 2006 Linear energy amplification in turbulent channels. *J. Fluid Mech.* **559**, 205–213.

del Álamo, J.C., Jiménez, J., Zandonade, P. & Moser, R.D. 2006 Self-similar vortex clusters in the turbulent logarithmic region. *J. Fluid Mech.* **561**, 329–358.

Baars, W.J. & Marusic, I. 2020*a* Data-driven decomposition of the streamwise turbulence kinetic energy in boundary layers. Part 1: energy spectra. *J. Fluid Mech.* **882**, A25.

Baars, W.J. & Marusic, I. 2020*b* Data-driven decomposition of the streamwise turbulence kinetic energy in boundary layers. Part 2: integrated energy and A_1. *J. Fluid Mech.* **882**, A26.

Baars, W.J., Squire, D.T., Talluru, K.M., Abbassi, M.R., Hutchins, N. & Marusic, I. 2016 Wall-drag measurements of smooth- and rough-wall turbulent boundary layers using a floating element. *Exp. Fluids* **57**, 90.

Chauhan, K.A., Monkewitz, P.A. & Nagib, H.M. 2010 Criteria for assessing experiments in zero pressure gradient boundary layers. *Fluid Dyn. Res.* **41**, 021404.

Cheng, C., Li, W., Lozano-Durán, A. & Liu, H. 2019 Identity of attached eddies in turbulent channel flows with bidimensional empirical mode decomposition. *J. Fluid Mech.* **870**, 1037–1071.

Cho, M., Hwang, Y. & Choi, H. 2018 Scale interactions and spectral energy transfer in turbulent channel flow. *J. Fluid Mech.* **854**, 474–504.

DESHPANDE, R., MONTY, J.P. & MARUSIC, I. 2020 Active and inactive components of the streamwise velocity in wall-bounded turbulence. *J. Fluid Mech.* **914**, A5.

DOOHAN, P., WILLIS, A.P. & HWANG, Y. 2019 Shear stress-driven flow: the state space of near-wall turbulence as $Re_\tau \to \infty$. *J. Fluid Mech.* **874**, 606–638.

ECKHARDT, B. & ZAMMERT, S. 2018 Small scale exact coherent structures at large Reynolds numbers in plane Couette flow. *Nonlinearity* **31**, R66–R77.

HELLSTÖM, L.H.O., MARUSIC, I. & SMITS, A.J. 2016 Self-similarity of the large-scale motions in turbulent pipe flow. *J. Fluid Mech.* **792**, R1.

HINCH, E.J. 1991 *Perturbation Methods*. Cambridge University Press.

HULTMARK, M., VALLIKIVI, M., BAILEY, S.C.C. & SMITS, A.J. 2012 On the logarithmic region in wall turbulence. *J. Fluid Mech.* **716**, R3.

HWANG, Y. 2015 Statistical structure of self-sustaining attached eddies in turbulent channel flow. *J. Fluid Mech.* **723**, 264–288.

HWANG, Y. 2016 Mesolayer of attached eddies in turbulent channel flow. *Phys. Rev. Fluids* **1** (6), 064401.

HWANG, Y. & BENGANA, Y. 2016 Self-sustaining process of minimal attached eddies in turbulent channel flow. *J. Fluid Mech.* **795**, 708–738.

HWANG, Y. & COSSU, C. 2010 Linear non-normal energy amplification of harmonic and stochastic forcing in the turbulent channel flow. *J. Fluid Mech.* **664**, 51–73.

HWANG, Y. & COSSU, C. 2011 Self-sustained processes in the logarithmic layer of turbulent channel flows. *Phys. Fluid* **23**, 061702.

HWANG, Y. & ECKHARDT, B.E. 2020 Attached eddy model revisited using a minimal quasilinear approximation. *J. Fluid Mech.* **894**, A23.

HWANG, Y. & LEE, M. 2020 The mean logarithm emerges with self-similar energy balance. *J. Fluid Mech.* **903**, R6.

HWANG, J. & SUNG, H.J. 2018 Wall-attached structures of velocity fluctuations in a turbulent boundary layer. *J. Fluid Mech.* **856**, 958–983.

HWANG, Y., WILLIS, A.P. & COSSU, C. 2016 Invariant solutions of minimal large-scale structures in turbulent channel flow for Re_τ up to 1000. *J. Fluid Mech.* **802**, R1.

JIMÉNEZ, J. & HOYAS, S. 2008 Turbulent fluctuations above the buffer layer of wall-bounded flows. *J. Fluid Mech.* **611**, 215–236.

JIMÉNEZ, J. & MOSER, R.D. 2007 What are we learning from simulating wall turbulence? *Phil. Trans. R. Soc.* A **365**, 715–732.

KLEWICKI, J.C. 2013 Self-similar mean dynamics in turbulent wall flows. *J. Fluid Mech.* **718**, 596–621.

LEE, M.K. & MOSER, R.D. 2015 Direct numerical simulation of turbulent channel flow up to $Re_\tau = 5200$. *J. Fluid Mech.* **774**, 395–415.

LOZANO-DURÁN, A. & JIMÉNEZ, J. 2014 Time-resolved evolution of coherent structures in turbulent channels: characterization of eddies and cascades. *J. Fluid Mech.* **759**, 432–471.

MARUSIC, I. & KUNKEL, G.J. 2003 Streamwise turbulent intensity formulation for flat-flate boundary layers. *Phys. Fluids* **15** (8), 2461.

MARUSIC, I. & MONTY, J.P. 2019 Attached eddy model of wall turbulence. *Annu. Rev. Fluid Mech.* **51**, 49–74.

MARUSIC, I., MONTY, J.P., HULTMARK, M. & SMITS, A.J. 2013 On the logarithmic region in wall turbulence. *J. Fluid Mech.* **716**, R3.

MATHIS, R., HUTCHINS, N. & MARUSIC, I. 2009 Large-scale amplitude modulation of the small-scale structures in turbulent boudnary layers. *J. Fluid Mech.* **628**, 311–337.

MCKEON, B.J. 2017 The engine behind (wall) turbulence: perspectives on scale interactions. *J. Fluid Mech.* **817**, P1.

MCKEON, B.J. 2019 Self-similar hierarchies and attached eddies. *Phys. Rev. Fluids* **4**, 082601(R).

MENEVEAU, C. & MARUSIC, I. 2013 Generalized logarithmic law for high-order moments in turbulent boundary layers. *J. Fluid Mech.* **719**, R1.

MOARREF, R., SHARMA, A.S., TROPP, J.A. & MCKEON, B.J. 2013 Model-based scaling of the streamwise energy density in high-Reynolds-number turbulent channels. *J. Fluid Mech.* **734**, 275–316.

MORRISON, J.F., JIANG, W., MCKEON, B.J. & SMITS, A.J. 2001 Reynolds number dependence of streamwise velocity spectra in turbulent pipe flow. *Phys. Rev. Lett.* **88** (21), 214501.

MORRISON, J.F., MCKEON, B.J., JIANG, W. & SMITS, A.J. 2004 Scaling of the streamwise velocity component in turbulent pipe flow. *J. Fluid Mech.* **508**, 99–131.

NICKELS, T.B., MARUSIC, I., HAFEZ, S. & CHONG, M.S 2005 Evidence of the $k-1$ law in a high Reynolds number turbulent boundary layer. *Phys. Rev. Lett.* **95**, 074501.

PERRY, A.E. & ABEL, J.C. 1977 Asymptotic similarity of turbulence structures in smooth- and rough-walled pipes. *J. Fluid Mech.* **79**, 785–799.

PERRY, A.E. & CHONG, M.S. 1982 On the mechanism of turbulence. *J. Fluid Mech.* **119**, 173–217.

PERRY, A.E., HENBEST, S. & CHONG, M.S. 1986 A theoretical and experimental study of wall turbulence. *J. Fluid Mech.* **165**, 163–199.

ROSENBERG, B.J., HULTMARK, M., VALLIKIVI, M., BAILEY, S.C.C. & SMITS, A.J. 2013 Turbulence spectra in smooth- and rough-wall pipe flow at extreme Reynolds numberss. *J. Fluid Mech.* **731**, 46–63.

SAMIE, M., MARUSIC, I., HUTCHINS, N., FU, M.K., FAN, Y., HULTMARK, M. & SMITS, A.J. 2018 Fully resolved measurements of turbulent boundary layer flows up to $Re_\tau = 20\,000$. *J. Fluid Mech.* **851**, 391–415.

SKOULOUDIS, N. & HWANG, Y. 2021 Scaling of turbulence intensities up to $Re_\tau = 10^6$ with a resolvent-based quasilinear approximation. *Phys. Rev. Fluids* **6**, 03460.

SREENIVASAN, K.R. & SAHAY, A. 1997 The persistence of viscous effects in the overlap region and the mean velocity in turbulent pipe and channel flows. In *Self-Sustaining Mechanisms of Wall Turbulence* (ed. R. Panton), pp. 253–272. Comp. Mech. Publ.

SRINATH, S., VASSILICOS, J.C., CUVIER, C., LAVAL, J.P., STANISLAS, M. & FOUCAUT, J.M. 2018 Attached flow structure and streamwise energy spectra in a turbulent boundary layer. *Phys. Rev.* E **97**, 053103.

TOWNSEND, A.A. 1956 *The Structure of Turbulent Shear Flow*, 1st edn. Cambridge University Press.

TOWNSEND, A.A. 1976 *The Structure of Turbulent Shear Flow*, 2nd edn. Cambridge University Press.

VADAREVU, S.B., SYMON, S., ILLINGWORTH, S.J. & MARUSIC, I. 2019 Coherent structures in the linearized impulse response of turbulent channel flow. *J. Fluid Mech.* **863**, 1190–1203.

VALLIKIVI, M., HULTMARK, M. & SMITS, A.J. 2015 Turbulent boundary layer statistics at very high Reynolds number. *J. Fluid Mech.* **779**, 371–389.

VALLIKIVI, M. & SMITS, A.J. 2014 Fabrication and characterization of a novel nanoscale thermal anemometry probe. *J. Microelectromech. Syst.* **23**, 899–907.

VASSILICOS, J.C., LAVAL, J.P., FOUCAUT, J.M. & STANISLAS, M. 2015 The streamwise turbulence intensity in the intermediate layer of turbulent pipe flow. *J. Fluid Mech.* **774**, 324–341.

VON KÁRMÁN, T. 1930 Mechanische aehnlichkeit und turbulenz. *Nachr. Ges. Wiss. Göttingen, Math. Phys. KL.*, 58–68, english translation NACA TM 611.

WEI, T., FIFE, P., KLEWICKI, J.C. & MCMURTRY, P. 2005 Properties of the mean momentum balance in turbulent boundary layer, pipe and channel flows. *J. Fluid Mech.* **522**, 303–327.

WOODCOCK, J.D. & MARUSIC, I. 2015 The statistical behaviour of attached eddies. *Phys. Fluids* **27**, 015104.

YANG, Q., WILLIS, A.P. & HWANG, Y. 2019 Exact coherent states of attached eddies in channel flow. *J. Fluid Mech.* **862**, 1029–1059.